Planar XY-model dynamics in a nematic liquid crystal system

Andrew N. Pargellis,[1] Susannah Green,[2] and Bernard Yurke[1]
[1] *AT&T Bell Laboratories, Murray Hill, New Jersey 07974*
[2] *Harvard University, Cambridge, Massachusetts 02138*
(Received 24 January 1994)

We have constucted a nematic liquid crystal system that exhibits the dynamics of a two-dimensional XY-model. The system consists of liquid crystal material placed between two sapphire windows coated with homeotropic alignment material. By holding the windows at two different temperatures, a thermal gradient can be maintained across the liquid crystal material such that the nematic-to-isotropic interface occurs at the center of the cell in a plane parallel to the two window surfaces. The boundary conditions that the interface and one of the windows impose on the nematic phase force the system's degrees of freedom to be those of the XY model. Comparison between experiment and numerical simulations indicate the system exhibits planar XY-model behavior.

PACS number(s): 61.30.Jf, 64.60.Cn, 05.70.Fh

When a system is rapidly quenched through a symmetry-breaking phase transition topological defects are produced. Following the quench the density of defects generally decreases with time. Often the growth of order for such systems exhibits self-similar scaling. In such cases the growth of order can be characterized by various scaling exponents. In particular, the growth of the correlation length $L(t)$ as a function of time t since the quench is characterized by the scaling exponent ϕ, $L(t) \sim t^{\phi}$. The spatial structure in the self-similar scaling regime is partially characterized by the scaling exponent μ which describes how the structure factor $S(q)$ scales for large transverse wave vector q, $S(q) \sim q^{-\mu}$. The rate at which memory of the initial conditions decays away is in part characterized by the scaling exponent $\bar{\lambda}$ which describes how the two-time correlation function $C(t, t_0)$ scales as a function of the correlation length $L(t)$ when t becomes large compared to t_0, $C(t, t_0) \sim L(t)^{-\bar{\lambda}}$. Recently, considerable theoretical effort [1, 2] has been devoted toward calculating these scaling exponents. Although there has been extensive work on the growth of order in systems possessing domain walls [3–5], only recently [6–13] has there been significant experimental work on systems containing topological defects with lower dimensionality. Most of the theoretical work has concentrated on systems with an n-dimensional vector order parameter, the so called O(n) models. Generally, the scaling exponents ϕ, μ, and $\bar{\lambda}$ depend on both the dimensionality n of the order parameter and the spatial dimensionality d of the system. One special case, $n = 2$ and $d = 2$, is called the planar XY model. Numerical simulations and theoretical predictions for ϕ and μ for this system indicate $\phi \leq 0.5$ [3, 14, 15] and $\mu = 4$[16, 17]. Only a $1/n$ expansion for $\bar{\lambda}$ exists and only two terms of this expansion have been evaluated [18]. To this order $\bar{\lambda} = 1.171$. The planar XY model is of particular interest because it has proven challenging to provide a rigorous theoretical description of the coarsening behavior for the system [19] and it has proven difficult to reach the self-similar scaling regime through numerical simulations [7–10,20–22] in order to extract reliable scaling exponents. It is thus of considerable interest to devise experimental systems exhibiting planar XY-model behavior with which one might measure the scaling exponents characterizing the coarsening. A thin film of smectic liquid crystal material which undergoes the smectic-A to smectic-C transition, in principle, would provide such a system. The xy degree of freedom is provided by the direction in which the director chooses to tilt. Previous work with smectic liquid crystals [8–10] so far has not resulted in suitable systems for measuring the scaling exponents for the XY model. Presumably, dislocations in smectic layers were responsible for the observed deviations from XY-model behavior. Lyotropic liquid crystal systems exhibiting a nematic phase have been used [12] to measure the scaling exponents ϕ and μ. The measured experimental values are consistent with the theoretical values given above. Because of the limited temperature range, low optical activity of the nematic phase, and the multicomponent nature of the liquid crystal material, these systems proved difficult to work with. Here we describe a thermotropic nematic liquid crystal system that is more convenient to work with and that does exhibit XY-model behavior as indicated by a comparison of the time evolution of the system with numerical simulations. This system was developed with the goal of measuring $\bar{\lambda}$. However, an initial bias in the director field has prevented us from attaining the self-similar scaling regime. Although this has prevented us from measuring $\bar{\lambda}$, the small bias required in simulations to fit the data indicates it should be possible to improve this system further and make such measurements in the future.

The system consists of nematic liquid crystal material placed between two sapphire windows as shown in Fig. 1. An axial thermal gradient through the liquid crystal material was maintained by holding the lower window at a higher temperature than the upper window. By a suitable choice of window temperatures the nematic-to-isotropic interface could be maintained near the center of the cell in a plane parallel to the windows. For

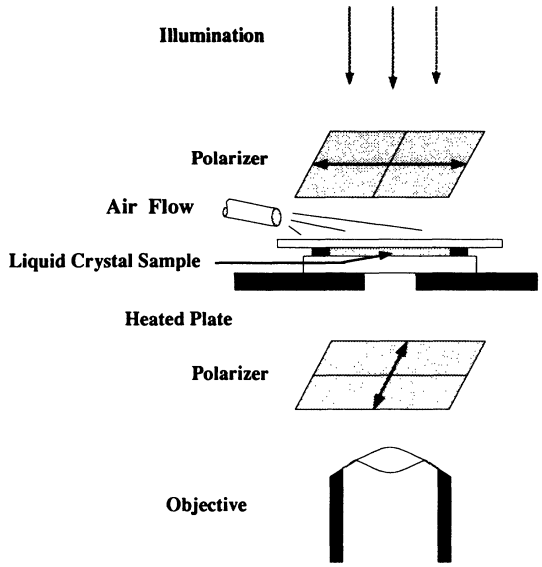

FIG. 1. Experimental arrangement.

the thermotropic liquid crystal material used, the director field (local molecular orientation) $\mathbf{n}$ for the nematic phase lies at an angle of 63.5° to the normal of the interface at the interface [31,32]. This provides the xy degree of freedom for the system. The upper sapphire window is coated with homeotropic alignment material, forcing the director to be perpendicular to the plane of the window. The defects in a planar XY-model system are pointlike and the order parameter has an integer winding number about the defect. Figure 2 shows an example of the structure of the defects for the present system. The defects in our system consist of halves of hedgehogs and hyperbolic hedgehogs whose singular points are at the nematic-to-isotropic interface. These defects are also referred to as "boojums" [23,33]. The structure of these

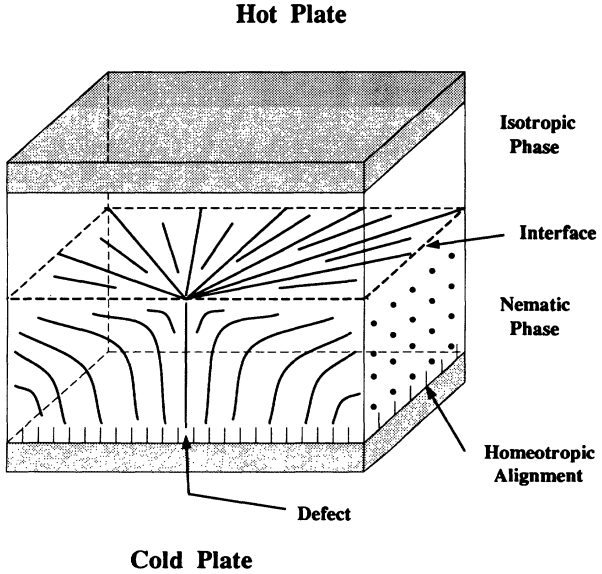

FIG. 2. Director configuration. For ease of depicting the configuration, this view is inverted from the actual experimental arrangement.

defects has been described by Lavrentovich and Nastishin [24, 25]. It should be noted that a nematic liquid crystal material does not distinguish between $\mathbf{n}$ and $-\mathbf{n}$ since the order parameter is a double-headed arrow (symmetric second rank tensor) rather than an arrow (vector) [26, 27]. However, because of the boundary conditions at the window surface and at the nematic-to-isotropic interface, this symmetry is effectively broken. That is, defects with a winding number of $\frac{1}{2}$ are not long-lived in this geometry. If present, a type $\frac{1}{2}$ disclination line would rapidly move to the interface and annihilate. The order parameter, which we take to be the director at the nematic-to-isotropic interface, is a vector of constant length, constrained to lie in a plane, as required for a system governed by XY-model dynamics. We will sometimes refer to this vector as a "spin vector" which is convenient terminology originally used for magnetic materials. A quench is induced by first heating both windows to a temperature sufficiently high that the liquid crystal material is in the isotropic phase throughout the sample cell. The temperature of the upper window is then suddenly reduced so that the resulting steady state temperature gradient maintains the nematic-to-isotropic interface at the center of the cell. Because of the finite size of the cell there is some three dimensionality at very early times after the quench. However, when the spacing between defects becomes comparable to the spacing between the windows the defect dynamics of the system crosses over to two-dimensional XY-model behavior.

The liquid crystal material used in the experiments reported here was 4-cyano-4′-n-pentylbiphenyl, known as K15 or 5CB. The spacing between the windows was 75 μm. The sample cell was heated from below with a resistively heated aluminum plate. The top window of the cell was a 1 mm thick sapphire disc with the standard 7° orientation for the optical axis and coated with a surfactant, N,N-dimethyl-N-octadecyl-3-aminopropyltrimethoxysilylchloride (DMOAP), that homeotropically aligns the director normal to the surface. The bottom window was a 3 mm thick, 0° sapphire disk. Sapphire was used because it is imperative to minimize radial thermal gradients (in the plane of the windows) in order that the isotropic-to-nematic interface be maintained near the center of the sample cell. The thermal conductivity of sapphire is about 40 $\mathrm{W\,m^{-1}K^{-1}}$, which is about 40 times that of glass. The top window was cooled with a controlled air stream, creating the thermal gradient along the axis. The time for the entire field of view (1.42 mm) to undergo the isotropic-to-nematic phase transition was $0.070 \pm .030$ sec. Earlier measurements with a similar sample cell [13] showed that the thermal quench occured at a rate of 0.3 °C/s. Using this number for the present set of experiments gives a radial thermal gradient on the order of $(dT/dt)(\Delta t/\Delta x) = (0.3)(0.070/1.42) = 0.015\,^{\circ}\mathrm{C/mm}$. Pointlike defects formed when a thermal quench forced the liquid crystal material at the upper window to go from the isotropic phase into the nematic phase. The defects were observed using an Olympus inverted microscope, illuminated from above with linearly polarized light. A Nikon M Plan 2.5/0.075 lens was employed. A

crossed polarizer between the sample cell and the objective allowed the incident linearly polarized light to be transmitted maximally when the director field was oriented at 45° to the polarizers. The strain field around a ± 1 defect thus appears as a cross ("schlieren pattern") with four dark brushes separated by four regions of maximal light transmission. A high speed color videorecorder (NAC Corp. Model HSV-400) was used to record the images at 200 frames per second.

The left-hand column of Fig. 3 shows a typical coarsening sequence with images taken from a sample area of 1.42×1.42 mm^2 at 30, 100, and 300 seconds. The video images have been processed so that the pixels are either black or white. The schlieren pattern clearly identifies the defects and shows they all have winding numbers of ± 1. From images such as these it is straightforward to measure the defect density. Apart from an arbitrary global rotation or reflection it is also possible to reconstruct the director field $\mathbf{n}(\mathbf{r}, t)$ from these schlieren images. We have performed such reconstructions in order to measure the time dependence of the two-time correlation function, $C(t, t_0)$, given by

$$C(t, t_0) = \langle \mathbf{n}(t) \cdot \mathbf{n}(t_0) \rangle = \langle \cos[\phi(t) - \phi(t_0)] \rangle, \quad (1)$$

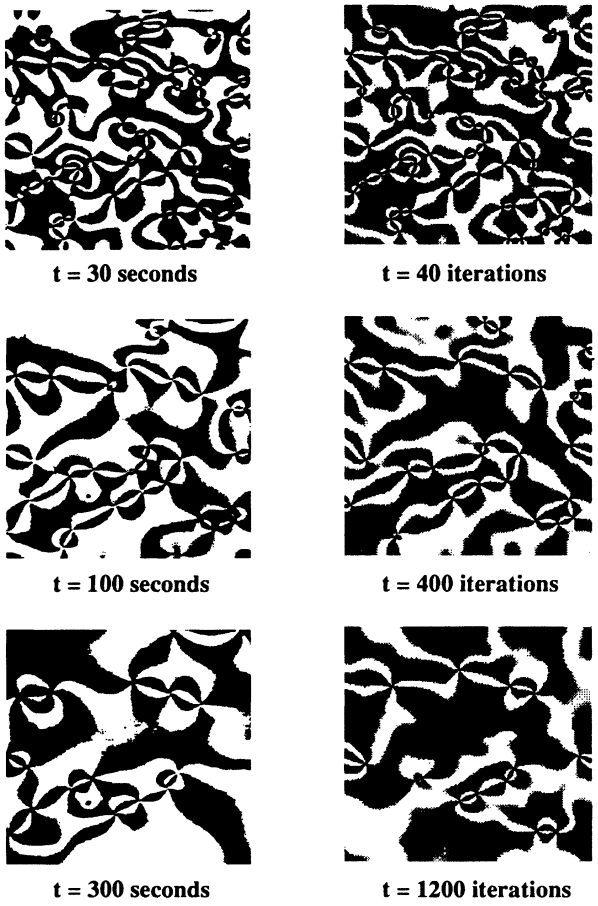

FIG. 3. Two coarsening sequences. Left-hand column: a single experimental run, 504; right-hand column: a single simulation using the 20 sec director field from run 504 as the initial condition. See text for a discussion on the generation of schlieren patterns.

where ϕ is the angle that the director $\mathbf{n}$ makes with respect to the x axis. The average is a spatial average. Although the director $\mathbf{n}$ varies smoothly, in our reconstructions of the director field only the octant of orientation of the director was determined. Schlieren patterns that have been saturated so that the pixels are either black or white are well suited for this kind of reconstruction. Numerical simulations showed that such a discretized approximation of the director field still gives an accurate measurement for $C(t, t_0)$.

The behavior of the system was compared with numerical simulations of an XY-model system governed [10] by the equation of motion

$$\gamma \frac{d\phi_i}{dt} = -\eta_i - \kappa \sum_j \sin(\phi_i - \phi_j) \ , \quad (2)$$

where i and j label lattice sites and ϕ_i is the angle that the spin vector at site i makes with respect to the x axis. Either square or triangular lattices were used, with the sum carried out over the nearest neighbors j surrounding a given lattice site i. The reorientational viscosity is denoted by γ and the coupling strength between nearest neighbor spins is given by κ. The Langevin noise η_i driving spin diffusion has zero mean and the moments

$$\langle \eta_i(t) \eta_j(t') \rangle = 2 k_B T \gamma \delta_{i,j} \delta(t - t'), \quad (3)$$

where k_B is Boltzmann's constant and T is the temperature of the heat bath responsible for the Langevin noise. This equation is numerically evaluated with the Euler update method [28]:

$$\phi_i(t + \Delta t) = \phi_i(t) - \Delta t \left\{ \eta_i(t) + \frac{\kappa}{\gamma} \sum_j \sin[\phi_i(t) - \phi_j(t)] \right\}, \quad (4)$$

where the constants κ and γ can arbitrarily be set equal to 1. The time is reported in number of time steps (iterations), M, where $t = M \Delta t$ is the dimensionless time. We used a time step of $\Delta t = 0.05$ which is half the maximum allowed by stability analysis of Eq. (4). No differences were observed in the defect dynamics when $\Delta t = 0.005$. At each time step the Langevin noise amplitudes $\eta_i(t) = 2\pi c_L r_i$ were generated by randomly selecting numbers r_i with a uniform distribution over the interval $[-0.5, 0.5]$. The amplitude of the Langevin noise is determined by the constant c_L. A value of $c_L = 2$ was used for the simulations reported here. This noise amplitude is well below the value $c_L = 3$ where a significant number of [29] short-lived defect pairs begin to be created. A value of $c_L = 2$ results in random fluctuations in the angle ϕ_i at each lattice site with an average of 9° every time step. The η_i thus have zero mean and the discretized version of Eq. (3) is

$$\langle \eta_i(m \Delta t) \eta_j(n \Delta t) \rangle = \frac{\pi^2}{3} c_L^2 \delta_{i,j} \delta_{m,n}, \quad (5)$$

where m and n are integers.

The simulations were performed on a variety of computers, and, unless stated otherwise, periodic boundary

conditions were employed. Most of our numerical simulations were done on a personal computer (Zeos Corp. Model 486) using a 100×100 array on a triangular lattice with the sum over the six nearest neighbors. This was sufficient to compare our simulations with experimental results over at least three decades in time. The finite-size effects, due to periodic boundary conditions, become noticeable after about 5000 iterations when there are fewer than ten defects and the correlation length ξ is comparable to the system size. Therefore, we ran some larger simulations with a 1024×1024 array, performed on a parallel processor machine containing 128×128 4-bit microprocessors (Model MP-1216D; MasPar Computer Corporation). It took eight hours of central processor time to perform $M = 10^5$ iterations. On the MasPar machine we used a square lattice array, summing in Eq. (4) over eight nearest neighbors. No differences in scaling have been observed using the two different geometries, but the triangular lattice initially allows for a denser network of defects. On the Zeos machine, defects were identified by going around each triangle in the array and checking to see if the director field rotated through $\pm2\pi$. On the Maspar machine, defect cores were identified by calculating the local strain energy $\mathcal{E}_i = \sum_j[1-\cos(\phi_i-\phi_j)]$ at each site i. If $\mathcal{E}_i$ exceeded a threshold value and was a local maximum at site i, the site was identified as a defect core. At times earlier than 30 iterations, when the defect density is high, this algorithm undercounts the number of defects by a factor of 2 when compared with the algorithm used on the Zeos 486 machine. For $M > 100$ iterations both algorithms were in excellent agreement with each other and only identified defects that were visually apparent in test images generated from the director field arrays.

The correlation function was determined, for simulations performed on the Zeos machine, from Eq. (1) by summing over all lattice positions i:

$$C(t,t_0) = \frac{1}{L^2}\sum_i \cos[\phi_i(t)-\phi_i(t_0)], \tag{6}$$

where $L = 100$ was the array size. The initial time is $t_0 = 1$ iteration.

In order to directly compare our experimental results with XY-model dynamics we ran a series of simulations which used as their initial conditions, not a random director field, but rather one obtained from experiment. We arbitrarily chose run 504 (out of nine possible runs). The video image at 20 sec was used to convert the black and white schlieren pattern into a director-field map. This map was then used as the initial condition. Figures 3–5 compare the experimentally attained visual images, defect densities, and correlation functions with those obtained by numerical integration. In all these figures, free boundaries were used instead of periodic boundaries for the numerical simulations. Figure 3 compares the results of the numerical simulations (right-hand column) with experiment (left-hand column). For comparison with experiment, the director field ϕ_i was displayed as a schlieren pattern by shading a pixel at site i white if the threshold, $\sin^2(2\phi_i) \approx 0.5$, was exceeded and black otherwise. The ϕ map was smoothed over nearest neighbors whenever generating an output image in order to display clearly the underlying schlieren pattern which would otherwise be very hard to see due to the Langevin agitation of the director field. The times for the right-hand column were 40, 400, and 1200 iterations.

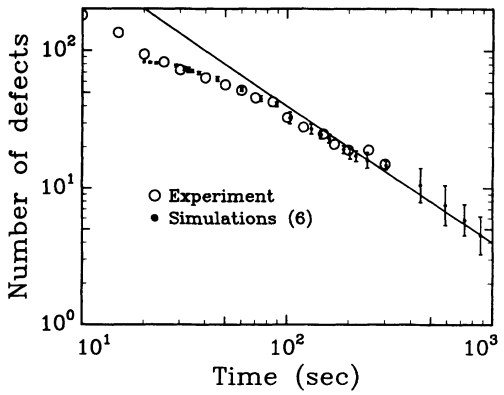

FIG. 4. Defect number versus time for run 504 (open circles) and averaged data for six simulations based on run 504 (error bars). The solid line shows the expected scaling $N(t) \propto t^{-1}$.

Figure 4 shows the decay in the number of defects $N(t)$ as a function of time for both the experimental data and numerical simulations. The late time scaling expected for the XY model, $N(t) \sim t^{-2\phi} \sim t^{-1}$, is shown by the solid line. The open circles are the data from run 504, counted over a region $(1.42)^2$ mm^2, and the dots with error bars are the averaged results from six simulations where the initial conditions were taken from run 504 at 20 sec and the simulation times (in iterations) are scaled to experimental times (in seconds) by the relation $t_{\rm sim} = 3.5t_{504} - 60$. This gave the best fit and is slightly different from the conversion used for the single run shown in Fig. 3, $t_{\rm sim} = 4t_{504} - 80$. The error bars indicate the variance in $N(t)$ which increases with time due to Langevin noise. Although the data follow the theoretically expected slope of -1 over approximately a decade, one can see that at late times the defects disappear faster that expected. Note that the experimental data and the numerical simulations, starting with the

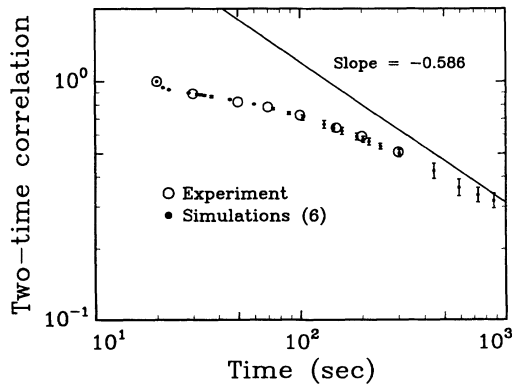

FIG. 5. Two-time correlation function for the same conditions discussed in Fig. 4. The slope of -0.586 for the solid line is that predicted by Bray and Humayun [1], for a scaling $C(t,t_0) \propto t^{-0.586}$.

same initial conditions at 20 sec, track each other well. Differences between the two are due to different boundary conditions and the Brownian motion of the defects, induced by the Langevin noise in the simulations.

Figure 5 depicts the two-time correlation function, $C(t,t_0)$, versus time for data from run 504 (open circles) and six simulations (dots with error bars). The late time scaling of the two-time correlation function expected for the XY model with uniform random initial conditions, $C(t,t_0) \sim t^{-\phi\bar{\lambda}} \sim t^{-0.585}$, is indicated by a solid line. Although our experimental data and numerical simulations do not enter the scaling regime, the experimental data and the numerical simulations track each other well.

The preceding three figures, which compare experiment with numerical simulations starting with the same initial conditions, demonstrate that the system is governed by XY model dynamics. That the experiment and the simulations do not exhibit the expected scaling behavior for the number density $N(t)$ or the two-time correlation function $C(t,t_0)$ indicates that some aspect of the initial director field is preventing the system from reaching a self-similar scaling regime. In order to evaluate the effect of a nonuniform probability distribution for the angle that the director field makes with respect to the x axis, we ran simulations with normalized probability distributions of the form

$$P(\phi) = \frac{1}{2\pi}[1 + A\cos(n\phi)] \,, \tag{7}$$

where A will be referred to as the bias parameter and n specifies the multipole character of the deviation of the probability distribution from a uniform distribution, $n = 1$ being dipolar, $n = 2$ being quadrupolar, etc. The construction of random number generators whose output ϕ has the probability distribution Eq. (7) is straightforward. In particular, if one has a random number generator outputing x such that the probability distribution $P(x)$ is uniform over the interval $[-0.5, 0.5]$, all one needs is a map $\phi(x)$ of x to the interval $[0, 2\pi]$ such that Eq. (7) holds. One way of accomplishing this is to assume that $\phi(x)$ is monotonic and demand that the total probability of generating a value in the subintervals $[0, x]$ and $[0, \phi(x)]$ be preserved

$$x = \int_0^x dx' = \int_0^{\phi(x)} P(\phi')d\phi' = \frac{\phi}{2\pi} + \frac{A}{2\pi n}\sin(n\phi). \tag{8}$$

This gives the transformation relation

$$2\pi x = \phi + \frac{A}{n}\sin(n\phi). \tag{9}$$

Since this equation does not yield a simple analytic expression for ϕ as a function of x, we used this equation to generate lookup tables to provide the mapping of x to ϕ.

The results of the simulations using these nonuniform probability distributions are shown in Figs. 6 and 7. Each sequence of data in Fig. 6 is a plot of the number of defects, averaged over at least ten runs, versus time. The solid line shows the expected asymptotic scaling of

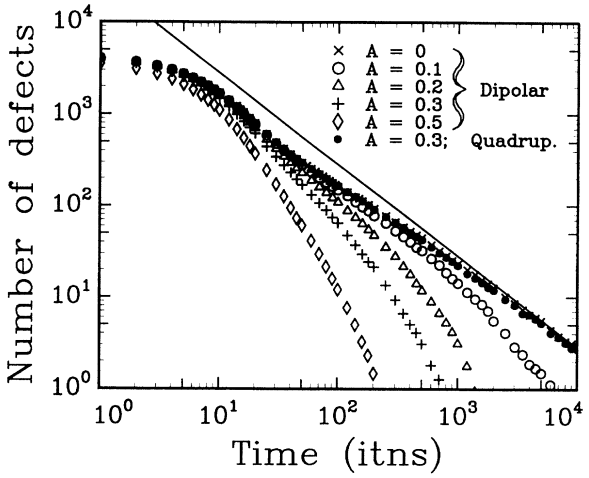

FIG. 6. The number of defects versus time in iterations obtained from computer simulations using Eq. (4) for different values of the bias parameter, A. The solid line has a slope of -1.0. The symbols and their respective values for the bias parameter A are shown in the inset.

the number of defects, $N(t) \propto t^{-1.0}$. The values of bias are all for a dipolar distortion from the uniform distribution, $n = 1$ in Eq. (7), except for the data shown by the solid circles which was quadrupolar with $n = 2$ and $A = 0.30$. The symbols are labeled in the inset, with values of A ranging from 0 to 0.5. A fit through the last decade of the zero-bias data gives the relationship $N(t) \propto t^{-\nu}$ with $\nu = 0.928 \pm .010$ for the decay of the defect density. This differs from the expected asymptotic scaling of t^{-1} because of logarithmic corrections due to the finite core size of the defects [10]. From Fig. 6 it is apparent that a dipolar distortion causes the defect density to decay more rapidly than t^{-1} scaling at late

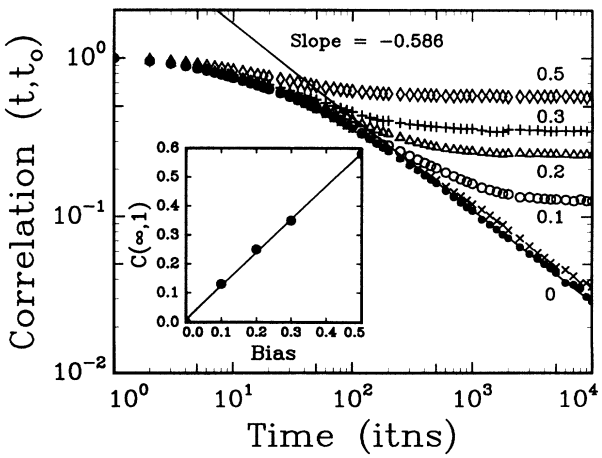

FIG. 7. The data of Fig. 6 but showing the time dependence of the two-time correlation function $C(t,1)$, as given in Eq. (6). The solid line has a slope of -0.585, as predicted by Bray and Humayun [1]. The symbols and values for the bias, A, are as in Fig. 6. The inset shows the linear relationship between the minimum value for the correlation function and the bias.

times. Note that the case $A = 0$ is indistinguishable from the case of a quadrupolar distortion with $A = 0.3$. In fact, the late time behavior of the decay of the defect density and the two-time correlation function is insensitive to distortions from a uniform distribution for the initial ϕ_i that involve only quadrupolar or higher distortions. This was verified through numerical simulations in which n of Eq. (7) ranged from 1–8 and A was chosen to be 0.3. The resulting curves for the number of defects and the two-time correlation function were indistinguishable from those obtained for a uniform distribution $A = 0$. For example, for the hexadecapolar distribution ($n = 8$) with a bias of $A = 0.3$, the number of defects is $N = 2.60 \pm 0.51$ at a time $t = 10^4$ iterations. This is within the statistical uncertainty of the defect number for no bias, $N = 2.97 \pm 0.28$. The respective two-time correlations differ slightly and are $C(10^4, 1) = 0.027$ and 0.036.

Figure 7 is the two-time correlation function plotted for various values of the bias parameter, A, for the same conditions as in Fig. 6. The symbols and values for A are the same as in Fig. 6. Both Figs. 6 and 7 show that the quadrupolar bias has no effect on the scaling of the defect number or correlation. The solid line has a slope of -0.586, the value predicted by Bray and Humayun [1] using the Mazenko model [2]. This is close to the scaling exponent extracted from the final decade for our zero-bias data, $\alpha = 0.543 \pm 0.009$. The inset shows the asymptotic values reached for the two-time correlation function as a function of bias and shows that the bias initially aligns a fraction of the director field in a preferred direction, that fraction resulting in the minimum value for $C(t, 1)$ for $t >> 1$.

In order to compare theory with experiment, we averaged the results for the defect density and the two-time correlation function as a function of time for nine experimental runs. In each experimental run we recorded the defect dynamics for a different area of the sample cell. In each case the area was $(1.42)^2$ mm^2. Figure 8 shows averaged values, on a logarithmic scale, of the defect number versus time for the nine experimental runs (solid circles) and at least 30 numerical simulations for each bias value, A. The numerical simulation data were rescaled to give the best fit to the experimental data, with $t_{\rm sim} = 17 t_{\rm expt}$ and $N_{\rm sim} = N_{\rm expt}/3.0$. The scaling factor in time is larger than used previously for the comparison with run 504 (17 versus 4) because these simulations were initiated from a random defect distribution with about 4000 defects initially. The defects scale with time as $N \ln N \propto t^{-1}$ and do not approach the asymptotic limit until several hundred iterations later, by which time the defect density is scaling similarly to the experimental data of 20 or 30 sec. The solid line has a slope of -1 indicating the expected scaling behavior for the defect number. Although the experimental data follow this line over the time interval from 20 to 200 seconds, it drops below the line both at short and at long times. The deficit of defects at early times is real and not due to an inability to resolve closely spaced defects. It is a measure of the number of defects generated at the quench time $t = 0$. This is partly determined by the growth rate of the nematic-to-isotropic

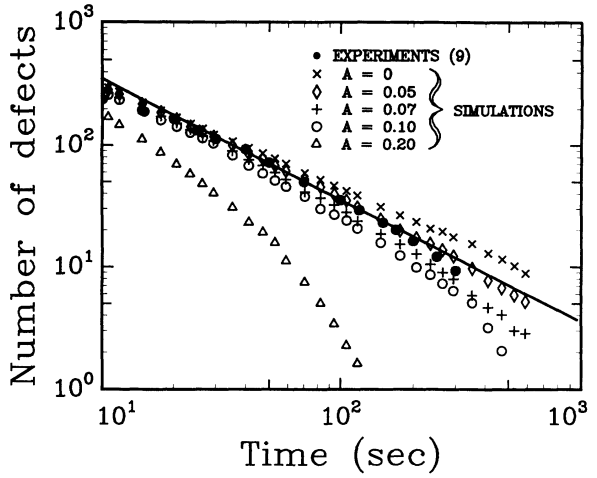

FIG. 8. Number of defects versus time, averaged for nine experimental runs (solid circles). The solid line is the expected $N \propto t^{-1}$ scaling. The results of the simulations, using Eq. (4), are shown for different values of the initial distribution bias parameter, A. The values for A are shown in the inset. The times are in seconds, with the scaling of iterations discussed in the text.

interface during the temperature quench. As discussed above, for the simulations the defect density as a function of time can be induced to decay away faster than t^{-1}, provided initial conditions are employed in which a dipolar component is present in the probability distribution for the ϕ_i. The symbols for the various values of A, ranging from 0 to 0.2, are defined in the inset. The simulations most closely follow the data points for a bias of $A = 0.07$. As an indication of the amount of initial director field bias, this comparison between experiment and theory should be regarded as qualitative rather than quantitative because logarithmic corrections to scaling, due to the finite core size of the defects, are still important for the numerical simulations [10].

In Fig. 9 the two-time correlation function $C(t, t_0)$ is

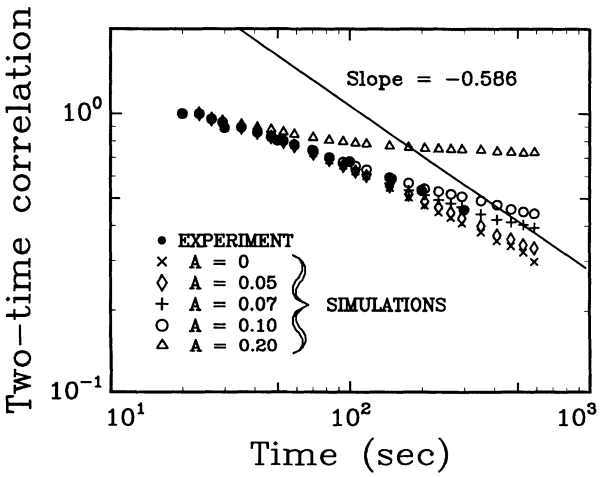

FIG. 9. As for Fig. 8 but showing the scaling of the two-time correlation function, $C(t, t_0)$. The correlations were determined in the simulations by the use of Eq. (6).

plotted for conditions similar to those for Fig. 8. The initial time is taken to be $t_0 = 20$ sec for the experimental data and $t_0 = 400$ iterations for the numerical simulations. The symbols and values for A are the same as in Fig. 4. The experimental values at late times exhibit a decay with an exponent, $\nu = 0.360 \pm 0.010$. As before, the best fit to the data is for a bias parameter $A = 0.07$. The solid line has a slope of -0.586 which the data do not follow.

For systems with a small initial bias in the order parameter, the growth of the "magnetization" provides a useful means of characterizing the growth of order [30]. For our system, the "magnetization" is given by

$$\mathbf{M(t)} = \frac{1}{N}\sum \mathbf{n}(\mathbf{r}, t), \tag{10}$$

where the sum is over position and N is the number of pixels (in a frame-grabbed image) or lattice sites. For small initial bias and sufficiently high initial defect density, the magnitude $M(t)$ of the magnetization is predicted to grow as

$$M(t) = |\mathbf{M}(t)| \propto L(t)^{\lambda} \tag{11}$$

at early times where $\lambda = d - \bar{\lambda} = 0.83$. Eventually, as the correlation length approaches the system size, the magnetization saturates. Thus, under suitable conditions, the scaling exponent $\bar{\lambda}$ can be determined from the slope of the curve obtained by plotting $M(t)/M(t_0)$ versus $L(t)/L(t_0)$ on log-log paper. Figure 10 compares the results of seven experimental runs with, for different values of initial bias, numerical simulations. The solid line has the predicted slope of 0.83. A least squares fit to the data obtained from the simulations with a bias of $A = 0.02$ over the time interval, $\log_{10}(t) = 0.3$ to 1.3, gives a slope of 1.060 ± 0.005 which is comparable to the predicted slope. In contrast, a least squares fit [from $\log(t) = 0.3$ to 1.3] for the experimental data gives a slope of $0.518 \pm .021$. The experimental data is thus in the "saturated magnetization" regime because the defects have been coarsening for 20 sec before we are able to analyze the data accurately. In fact, following the procedure discussed above, if we rescale the numerical simulation data by choosing $M(t_0)$ and $L(t_0)$ at time $t_{0,\mathrm{sim}} = 17 t_{0,\mathrm{expt}} = 350$, we get the saturated magnetization results shown in Fig. 11. The experimental data are in good agreement with the shifted numerical data for the optimum bias value $A = 0.07$ used to fit the experimental data shown in Figs. 8 and 9.

Comparison of numerical simulations with the experiments indicate the presence of a bias in the initial director field. The source for this initial bias is unknown. The air flow cooling process generates small thermal gradients, hence during a quench the nematic phase first appears in a few patches which then grow and fill the entire field of view. It is possible that this directional propagation of the nematic-to-isotropic interface gives rise to a preferential bias in the initial director field. It is also possible that some preferential alignment in the homeotropic alignment material is responsible for the initial director field bias. The quality of the alignment material is sensitive to preparation conditions. For example, if a droplet of water was rolled across the cell window after application of the homeotropic alignment material, then a bare streak, devoid of defects, was observed for most of the experimental run. Any defects that formed during the thermal quench in these affected areas rapidly annealed away in a few seconds, indicating the alignment material had been affected. However, the absence of confinement effects of the type seen in smectics [8] indicates that a preferential alignment in the homeotropic alignment material, if present, is not strong enough to produce confinement on the length scales of the present experiment.

In conclusion, a nematic liquid crystal system has been constructed that exhibits the defect dynamics of a two-dimensional XY model. This is verified by using the early-time director field from experimental runs as initial conditions for the numerical simulation runs. The defect number $N(t)$ and two-time correlation function $C(t, t_0)$ then track each other very well for later times. The nonscaling of $N(t)$ and $C(t, t_0)$ can be explained by a preferential bias in the initial director field. Numer-

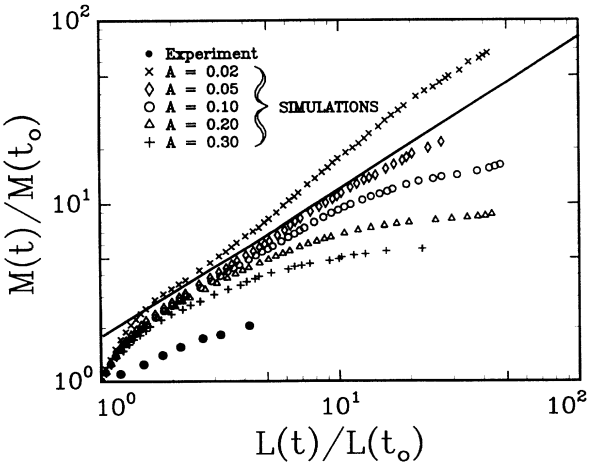

FIG. 10. Net director orientation (magnetization) as a function of normalized correlation length for different bias values A. The solid line has the predicted slope as given in Eq. (11) with $\lambda = 0.83$.

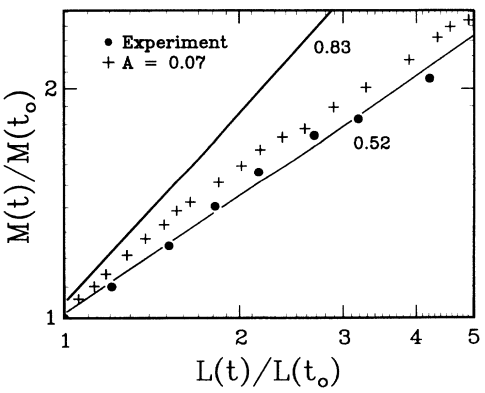

FIG. 11. As for Fig. 10 but with the numerical simulation data rescaled as discussed in the text. Both lines are labeled with their respective slopes.

ical simulations with a biased initial probability distribution exhibit coarsening in good agreement with the experimentally observed values. In addition, the magnetization $M(t)/M(t_0)$ versus correlation length $L(t)/L(t_0)$ indicates the experimental data are in the saturated magnetization regime in a system with a bias in the initial distribution for the director field. More careful sample preparation may enable one to reduce the preferential bias in the initial conditions sufficiently so that the scaling regimes can be attained.

We gratefully acknowledge useful discussions on the material properties of liquid crystals with Frank V. Allan. Terry Kovacs was responsible for the original generation of the programs used on the MasPar and generously assisted us in altering the programs whenever system modifications required it. We also thank Alan J. Bray for fruitful discussions on the scaling theory.

[1] A. J. Bray and K. Humayun, J. Phys. A **25**, 2191 (1992).
[2] G. F. Mazenko, Phys. Rev. Lett. **63**, 1605 (1989).
[3] S. M. Allen and J. W. Cahn, Acta Metall. **27**, 1085 (1979).
[4] J. D. Gunton, M. San Miguel, and P. S. Sahni, in *Phase Transitions and Critical Phenomena*, edited by C. Domb and J. L. Lebowitz (Academic, London, 1983).
[5] *Dynamics of Ordering Processes in Condensed Matter*, edited by S. Komura and H. Furukawa (Plenum, New York, 1988).
[6] T. Shiwaku, A. Nakai, H. Hasegawa, and T. Hashimoto, Polym. Commun. **28**, 174 (1987); Macromolecules **23**, 1590 (1990).
[7] I. Chuang, Master's thesis, M. I. T., 1991.
[8] A. N. Pargellis, P. Finn, J. W. Goodby, P. Panizza, B. Yurke, and P. E. Cladis, Phys. Rev. A **46**, 7765 (1992).
[9] C. D. Muzny and N. A. Clark, Phys. Rev. Lett. **68**, 804 (1992).
[10] B. Yurke, A. N. Pargellis, T. Kovacs, and D. A. Huse, Phys. Rev. E **47**, 1525 (1993).
[11] A. P. Y. Wong, P. Wiltzius, and B. Yurke, Phys. Rev. Lett. **68**, 3583 (1992).
[12] A. P. Y. Wong, P. Wiltzius, R. G. Larson, and B. Yurke, Phys. Rev. E **47**, 2683 (1993).
[13] N. Mason, A. N. Pargellis, and B. Yurke, Phys. Rev. Lett. **70**, 190 (1993).
[14] H. Toyoki, Mod. Phys. Lett. B **7**, 397 (1993).
[15] R. E. Blundell and A. J. Bray, Phys. Rev. A **46**, R6154 (1992).
[16] A. J. Bray and S. Puri, Phys. Rev. Lett. **67**, 2670 (1991).
[17] F. Liu and G. F. Mazenko, Phys. Rev. B **45**, 6989 (1992).
[18] T. J. Newman and A. J. Bray, J. Phys. A. **23**, 4491 (1990).
[19] A. J. Bray, in *Phase Transitions and Relaxation in Systems with Competing Energy Scales*, Vol. 415 of *NATO Advanced Study Institute Series C: Mathematical and Physical Sciences*, edited by T. Riste and D. Sherrington (Kluwer, Boston, 1993).
[20] M. Mondello and N. Goldenfeld, Phys. Rev. A **42**, 5865 (1990).
[21] H. Toyoki, Phys. Rev. A **42**, 911 (1990).
[22] R. Loft and T. A. DeGrand, Phys. Rev. B **35**, 8528 (1987).
[23] M. V. Kurik and O. D. Lavrentovich, Usp. Fiz. Nauk. **154**, 381 (1988) [Sov. Phys. Usp. **31**, 196 (1988)].
[24] O. D. Lavrentovich and Y. A. Nastishin, Europhys. Lett. **12**, 135 (1990).
[25] O. D. Lavrentovich, Phys. Scr. **T39**, 394 (1991).
[26] P. G. de Gennes, *The Physics of Liquid Crystals* (Oxford University Press, London, 1974).
[27] N. D. Mermin, Rev. Mod. Phys. **51**, 591 (1979).
[28] D. Potter, *Computational Physics* (John Wiley, London, 1973), p. 37.
[29] J. M. Kosterlitz and D. J. Thouless, J. Phys. C **6**, 1181 (1973).
[30] J. G. Kissner and A. J. Bray, J. Phys. A **25**, 31 (1992).
[31] S. Faetti and V. Palleschi, Phys. Rev. A **30**, 324 (1984).
[32] M. J. Bowick, L. Chandar, E. A. Schiff, A. M. Srivastava, Science **263**, 943 (1994).
[33] R. B. Meyer, Mol. Cryst. Liq. Cryst. **16**, 355 (1972).

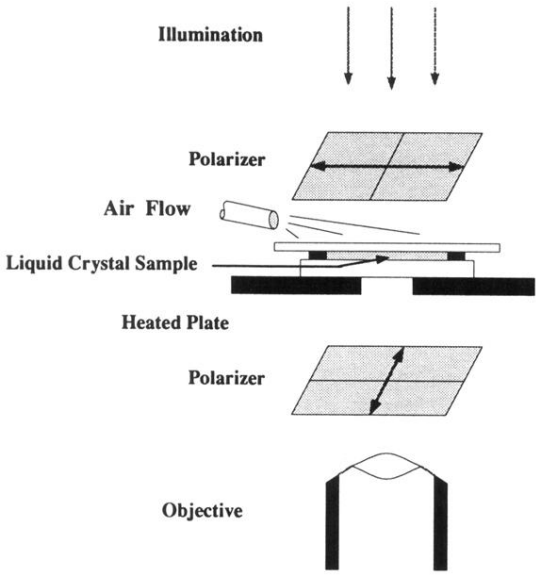

FIG. 1. Experimental arrangement.

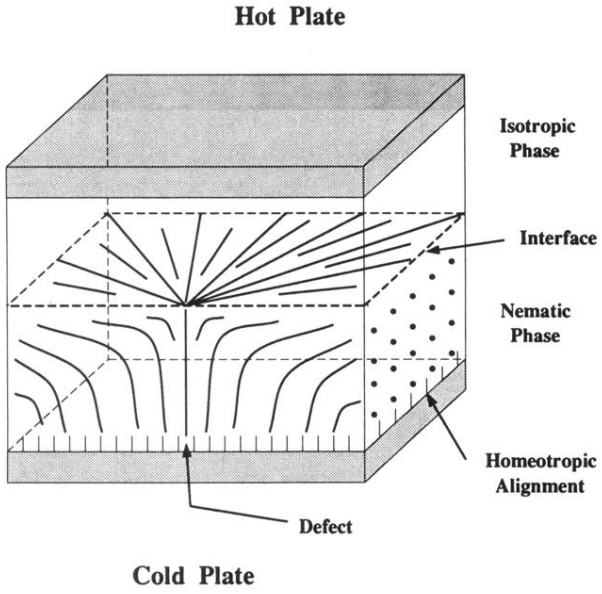

FIG. 2. Director configuration. For ease of depicting the configuration, this view is inverted from the actual experimental arrangement.

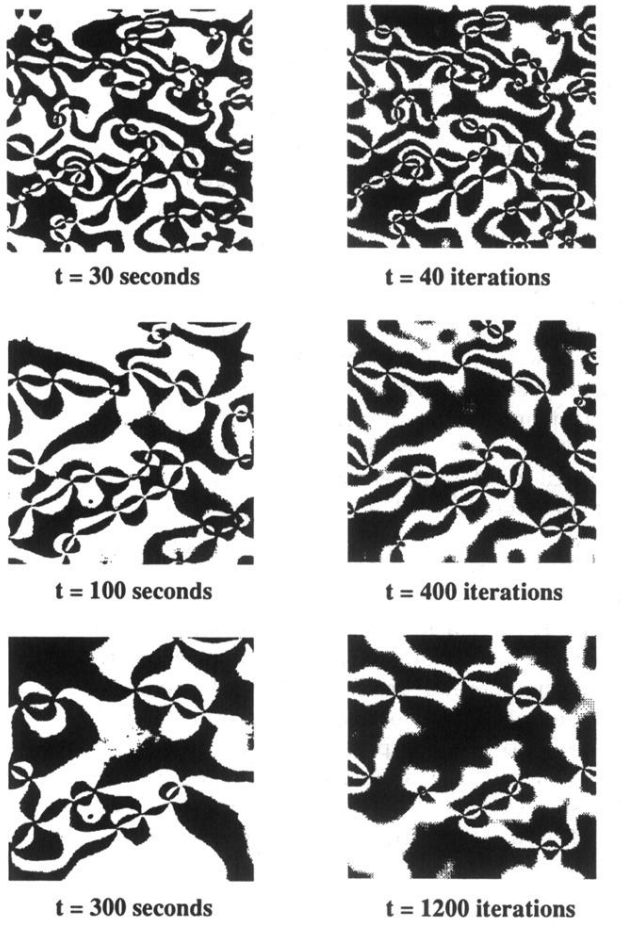

FIG. 3. Two coarsening sequences. Left-hand column: a single experimental run, 504; right-hand column: a single simulation using the 20 sec director field from run 504 as the initial condition. See text for a discussion on the generation of schlieren patterns.